XLIII CILAMCE
21–25, November, 2022
FOZ DO IGUAÇU – PR – BRAZIL

Nonlinear Dynamic Analysis of Composite Laminate Plates Subjected to Explosive Loading

Ana Waldila de Queiroz Ramiro Reis[1], Rodrigo Bird Burgos[1,2]

[1]*Civil Engineering Post Graduate Program, Rio de Janeiro State University*
anawaldila@hotmail.com
[2] *Department of Structures and Foundations, Rio de Janeiro State University*
Rua São Francisco Xavier, 524, Rio de Janeiro, Brazil
rburgos@eng.uerj.br

Abstract. Explosive loads have been the target of study in recent years due to the catastrophic effects that this type of loading can cause in civil engineering structures. This phenomenon is characterized by the release of energy in short time intervals, causing a peak of overpressure and, in sequence, a suction process, or overpressure. Due to the high impact, this episode can generate catastrophic effects on structures, such as partial or total collapse, and in severe cases, several deaths. At the same time, laminated plates are structural elements that are being studied for their characteristic of improving the physical properties of the primary materials used in their composition. Thus, this work aims to present a study on laminated plates, present in literature, subjected to blast loads to reproduce the results. In the sequence, an evaluation of their behavior when the negative phase is not considered is verified, to understand how this portion of the loading influences the final behavior of the structure. Finally, a parametric study of the laminated plates is performed to determine, for each structure, equations of correlation between the maximum displacement obtained by the structure and characteristic parameters of the shock wave. In the calculation process, for each example present in the literature, a plate theory is used, considering second-order effects. The differential equations are obtained according to the Total Minimum Potential Energy, in their solution, the Galerkin method is employed, and, finally, to obtain the displacements the Runge-Kutta numerical method is used.

Keywords: laminated plates, blast load, von Karman theory.

1 Introduction

Many studies have been realized about the behavior of laminated plate structures in static and dynamic analysis, based on the versatility of application in several areas, such as civil, mechanical, and aeronautical engineering, among others. However, the result of dynamic behavior has been the focus of research, especially for cases of extreme loads, such as explosions.

Composite laminated plates are formed by a set of layers, which can be treated according to the prerogatives of Kirchhoff or Mindlin methodologies. In addition of that, the explosion phenomenon corresponds to a rapid release of energy from an explosive source. The first recorded studies of the explosion phenomenon are realized by Friedlander [1], who suggested a simple formula to characterize blast waves. Granström [2] recorded studies on the best negative phase equation. Subsequently, the US Department of Defense [3] presented a complete manual of the mathematical characterization of the blast wave. Rigby et al. [4] and Rigby [5] use the abacus provided by the US Department of Defense [3] to characterize the curves and convert them to the SI.

Studies of single and multi-laminar plates were also a focus for the explosive loads consideration. Gupta [6] presented an analysis with a mathematical formulation of a thin plate, considering only the positive phase in the blast wave. Librescu and Nosier [7] presented analyzes of laminated plates subjected to explosive charges and sonic explosions. Wei and Dharani [8] realized studies related to laminated sandwich plates, in which layers are made of glass and the core of PVB (polyvinyl butyral). Kazanci and Mecitoglu [9] consider the nonlinear behavior of the plates and consider the Friedlander equation as the explosive load. Susler et al. [10] applied explosive load

to laminated plates with thickness variation. Amabili et al. [11] studied the behavior of a laminated glass plate considering the nonlinear geometric effect on the structure. The American Society of Civil Engineers (ASCE [12]) has published a document referring to structures in general subjected to explosive charges. Reis [13], Reis et al. [14] and Reis et al. [15] presented a study of thin plates subjected to explosive loads considering the use of Single Degree of Freedom (SDOF). Reis et al. [15] presented examples from the literature and compared the results for the explosion equated by the cubic polynomial, thus emphasizing the difference in results in the maximum displacement of the structure when comparing the use of the negative phase with the using only the positive phase.

2 Methodology

2.1 Laminated Plate

According to Reddy [16] and Mendonça [17], composite materials are formed by at least two materials that, on a macroscopic scale, have better properties than conventional materials, when analyzed individually, would not be able to obtain the same properties as needed. Composite laminates correspond to layers of different materials, each one usually formed by fibers, which orientation will define the resistance capacity and improve the mechanical properties of the structure, as shown in Fig. 1.

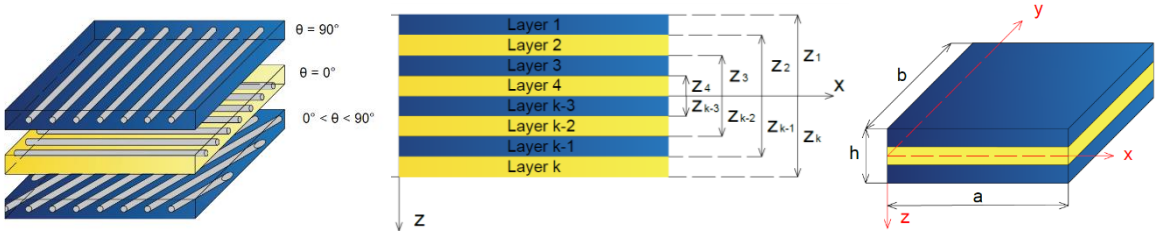

(a) (b) (c)

Figure 1. (a) Composite laminated plate, (b) Transversal section in laminated plate, (c) Global axes in structure

2.2 Strain-Displacement Relations

It is considered a rectangular plate of length a, width b and height h, composed of k layers of location of its upper fibers z_i each, as shown in Fig. 1. The main theories of laminated plates are given by the Classical Laminated Plates Theory (CLPT), Classical Laminate Plate Theory – von Kárman (TvK), First Order Laminated Plate Shear Theory (FSPT) and High Order Laminated Plate Shear Theory (HSPT), as presented by Reddy [16]. For this, the displacements are represented according to Equation (1).

$$\begin{aligned} u(x,y,z) &= u_0(x,y) + z\left[\alpha_1 \frac{\partial w_0}{\partial x} + \alpha_2 \theta_x + \alpha_3 z^2 \left(\theta_x + \frac{\partial w_0}{\partial x}\right)\right], \\ v(x,y,z) &= v_0(x,y) + z\left[\alpha_1 \frac{\partial w_0}{\partial y} + \alpha_2 \theta_y + \alpha_3 z^2 \left(\theta_y + \frac{\partial w_0}{\partial y}\right)\right], \\ w(x,y,z) &= w_0(x,y), \end{aligned} \tag{1}$$

where u, v, and w are displacements in directions x, y, and z, respectively, u_0, v_0 and w_0 are the midpoint displacements in directions x, y e z, respectively, θ_x and θ_y are the rotations of a transversal normal about the y- and x-axis, respectively, and α_i is an auxiliary parameter, presented in Tab. 1. Regarding the strain-displacement relation, Equation (2) shows a general expression considering the plate theories mentioned previously.

$$\begin{Bmatrix} \varepsilon_{xx} \\ \varepsilon_{yy} \\ \gamma_{xy} \end{Bmatrix} = \begin{Bmatrix} \varepsilon_{xx}^{(0)} \\ \varepsilon_{yy}^{(0)} \\ \gamma_{xy}^{(0)} \end{Bmatrix} + z \begin{Bmatrix} \kappa_{xx}^{(1)} \\ \kappa_{yy}^{(1)} \\ \kappa_{xy}^{(1)} \end{Bmatrix} + z^3 \begin{Bmatrix} \kappa_{xx}^{(3)} \\ \kappa_{yy}^{(3)} \\ \kappa_{xy}^{(3)} \end{Bmatrix}, \begin{Bmatrix} \gamma_{yz} \\ \gamma_{xz} \end{Bmatrix} = \begin{Bmatrix} \gamma_{yz}^{(0)} \\ \gamma_{xz}^{(0)} \end{Bmatrix} + z^2 \begin{Bmatrix} \gamma_{yz}^{(2)} \\ \gamma_{xz}^{(2)} \end{Bmatrix}, \tag{2}$$

where ε_{xx}, ε_{yy}, and ε_{xz} are the bending strains, γ_{yz} and γ_{xz} are the transverse shear strains, $\varepsilon^{(0)}{}_{ij}$ are the middle surface strain, $\kappa^{(1)}{}_{ij}$ and $\kappa^{(3)}{}_{ij}$ are the flexural bending strains (curvatures), $\gamma^{(0)}{}_{ij}$ and $\gamma^{(2)}{}_{ij}$ are the first and high order of transverse shear strain, respectively, as presented by Reddy [16].

Table 1. α_i values

Theory	α_1	α_2	α_3
CLPT	-1	0	0
FSPT	0	1	0
TSPT	0	1	$-4/(3h^2)$
TvK	-1	0	0

2.3 Constitutive Relations

Considering that the material is orthotropic, with k layers present in the plate, and according to Mendonça [17], the structure is under plane stresses state, the stiffness parameters are present by Equation (3):

$$\begin{Bmatrix} \sigma_1^l \\ \sigma_2^l \\ \tau_{12}^l \end{Bmatrix}^{(k)} = \begin{bmatrix} Q_{11} & Q_{12} & 0 \\ Q_{12} & Q_{22} & 0 \\ 0 & 0 & Q_{66} \end{bmatrix}^{(k)} \begin{Bmatrix} \varepsilon_1^l \\ \varepsilon_2^l \\ \gamma_{12}^l \end{Bmatrix}^{(k)}, \begin{Bmatrix} \tau_{23}^l \\ \tau_{13}^l \end{Bmatrix}^{(k)} = \begin{bmatrix} Q_{44} & 0 \\ 0 & Q_{55} \end{bmatrix}^{(k)} \begin{Bmatrix} \gamma_{23}^l \\ \gamma_{23}^l \end{Bmatrix}^{(k)},$$
$$Q_{11}^{(k)} = \frac{E_1^{(k)}}{1-\nu_{12}^{(k)}\nu_{21}^{(k)}}, \quad Q_{12}^{(k)} = \frac{\nu_{12}^{(k)}E_2^{(k)}}{1-\nu_{12}^{(k)}\nu_{21}^{(k)}}, \quad Q_{22}^{(k)} = \frac{E_2^{(k)}}{1-\nu_{12}^{(k)}\nu_{21}^{(k)}}, \quad Q_{66}^{(k)} = G_{12}^{(k)}, \quad Q_{44}^{(k)} = G_{23}^{(k)}, \quad Q_{55}^{(k)} = G_{13}^{(k)}, \tag{3}$$

where σ^l_i and τ^l_{ij} are the bending stress and shear tensile for each layer, [Q] is the stiffness matrix of each layer (local system), ε^l_i and γ^l_{ij} are the bending strain and shear strain of each layer, E_i is the Young's Modulus in *i* axis, ν_{ij} is the Poisson rate, G_{ij} is the shear modulus. For the global system, Equation (4) shows:

$$\begin{Bmatrix} \sigma_{xx} \\ \sigma_{yy} \\ \tau_{xy} \end{Bmatrix}^{(k)} = \begin{bmatrix} \bar{Q}_{11} & \bar{Q}_{12} & \bar{Q}_{16} \\ \bar{Q}_{12} & \bar{Q}_{22} & \bar{Q}_{26} \\ \bar{Q}_{16} & \bar{Q}_{26} & \bar{Q}_{66} \end{bmatrix}^{(k)} \begin{Bmatrix} \varepsilon_{xx} \\ \varepsilon_{yy} \\ \gamma_{xy} \end{Bmatrix}^{(k)}, \begin{Bmatrix} \tau_{yz} \\ \tau_{xz} \end{Bmatrix}^{(k)} = \begin{bmatrix} \bar{Q}_{44} & \bar{Q}_{45} \\ \bar{Q}_{45} & \bar{Q}_{55} \end{bmatrix}^{(k)} \begin{Bmatrix} \gamma_{xy} \\ \gamma_{xz} \end{Bmatrix}^{(k)}, \tag{4}$$

where σ_{ij}, τ_{ij}, $[\bar{Q}]$, ε_{ij}, and γ_{ij} are global bending and shear stresses, global stiffness matrix, and global bending and shear strains, respectively. All expressions to obtain $[\bar{Q}]$ can be verified in Reddy [16] and Mendonça [17].

2.4 Governing Equations

The process of obtaining the governing equations corresponds to that used by Reddy [16], considering Hamilton's principle, represented by Equation (5).

$$\delta\int_{t_1}^{t_2}(U-K+W)\,dt = 0, \tag{5}$$

where *U*, *K*, and *W* are the strain, kinetic, and work energies, respectively, as Equations (6) to (8).

$$\delta U = \frac{1}{2}\int_A\int_z \left(\sigma_{xx}\delta\varepsilon_{xx} + \sigma_{yy}\delta\varepsilon_{yy} + \tau_{xy}\delta\gamma_{xy} + \tau_{yz}\delta\gamma_{yz} + \tau_{xz}\delta\gamma_{xz}\right)dzdA, \tag{6}$$

$$\delta K = \frac{1}{2}\int_A\int_z \rho_0\left(\dot{u}\delta\dot{u} + \dot{v}\delta\dot{v} + \dot{w}\delta\dot{w}\right)dzdA, \tag{7}$$

$$\delta W = \int_A q_0\delta w_0 dA, \tag{8}$$

where ρ_0 and q_0 are the density of the material and the external load applied, respectively.

2.5 Solution

Based on Reddy [16], was presented the process for cross-ply plates, classified as SS1, and angle-ply, given by SS2, represented simply supported plates. Expressions for cross-ply plates are presented in Equation (9).

$$u_0(x,y,t)=\sum_{n=1}^{\infty}\sum_{m=1}^{\infty}U_{mn}(t)\cos\left(\frac{\pi m}{a}x\right)\sin\left(\frac{\pi n}{b}y\right),\quad \phi_x(x,y,t)=\sum_{n=1}^{\infty}\sum_{m=1}^{\infty}X_{mn}(t)\cos\left(\frac{\pi m}{a}x\right)\sin\left(\frac{\pi n}{b}y\right),$$
$$v_0(x,y,t)=\sum_{n=1}^{\infty}\sum_{m=1}^{\infty}V_{mn}(t)\sin\left(\frac{\pi m}{a}x\right)\cos\left(\frac{\pi n}{b}y\right),\quad \phi_y(x,y,t)=\sum_{n=1}^{\infty}\sum_{m=1}^{\infty}Y_{mn}(t)\sin\left(\frac{\pi m}{a}x\right)\cos\left(\frac{\pi n}{b}y\right), \tag{9}$$
$$w_0(x,y,t)=\sum_{n=1}^{\infty}\sum_{m=1}^{\infty}W_{mn}(t)\sin\left(\frac{\pi m}{a}x\right)\sin\left(\frac{\pi n}{b}y\right),$$

where U_{mn}, V_{mn}, W_{mn}, $X_{mn,}$ and Y_{mn} are Fourier's series parameters and m,n = 1,3,5...

The process for both cases is the same, the difference is given by the displacement equations applied, which one for the SS2 case there is a difference only in the expressions of u_0 and v_0, i.e., $u_0 = \sum\sum U_{mn}(t)\sin(\pi mx/a)\cos(\pi nx/b)$ and $v_0 = \sum\sum V_{mn}(t)\cos(\pi mx/a)\sin(\pi nx/b)$. Applying the Fourier series, represented by Equation (9), in Equation (5), the differential system of equations to be solved is observed in Equation (10):

$$[M]\{\ddot{\Delta}\}+[C]\{\dot{\Delta}\}+\left([K]+N_2(\Delta)+N_3(\Delta,\Delta)\right)\{\Delta\}=\{F\},$$
$$\{\Delta\}=\{U_{mn}(t)\quad V_{mn}(t)\quad W_{mn}(t)\quad X_{mn}(t)\quad Y_{mn}(t)\}^T, \tag{10}$$

where [M], [C], and [K], are the mass matrix, damping matrix and stiffness matrix of the structure, respectively, $N_2(\Delta)$ and $N_3(\Delta, \Delta)$ are matrices of first and second-degree functions of the parameters of the Fourier series present in Equation (9) and {F} is the vector of forces. The solution of Equation (10) is given according to the numerical method of Runge-Kutta since it is a highly nonlinear equation.

2.6 Explosive Load

Blast waves correspond to a rapid release of energy from an explosive source. When this wave reaches a bulkhead, an overpressure peak, p_{max}, is generated, which decays exponentially according to the decay coefficient, *a*', until zero pressure, at time t_d, which is the duration of the positive phase. Then, the negative phase begins, reaching a maximum under pressure, p_{min}. Finally, this pressure gradually increases until it once again reaches the value of zero, when the load application ends, whose duration of this phase is t^-_d (Reis et al. [15]). The blast wave behavior is present in Rigby et al. [4], Reis [13], Reis et al. [14], and Reis et al. [15]. The characterization of the curve was studied by Friedlander [1] and Granström [2], who elaborated the equations of the positive and negative phases, respectively, according to Equation (11). In addition, it is important to notice that all parameters present in Equation (11) are determined in this work according to the US Department of Defense [3] abacus, which is directly related to the parameter Z, scaled distance, given in Equation (12). Also, for the example presented in this work, the blast wave equation is applied using the expanded Friedlander equation. In other words, the Friedlander equation was used for both positive and negative phases.

$$p(t)=\begin{cases} p_{\max}\left(1-\dfrac{t}{t_d}\right)e^{-\frac{a't}{t_d}} & ,t\le t_d \\ -p_{\min}\left(\dfrac{6.75(t-t_d)}{t_d^-}\right)\left(1-\dfrac{(t-t_d)}{t_d^-}\right)^2 & ,t_d\le t\le t_d+t_d^- \end{cases}, \tag{11}$$

$$Z=\frac{R}{\sqrt[3]{W_{TNT}}}, \tag{12}$$

where R is the distance between the explosive source and the plate and W_{TNT} is the explosive mass.

3 Results

Considering that in the literature there are some examples of plates subjected to explosive loads, specific for each case, this work improves the evaluation of one example of a structure through parametric analysis of the loading used. In other words, demonstrate how the structure performs, the maximum displacement of the structure (u_z/h), by varying the parameters of Z (scaled distance) and W_{TNT}, to develop its general displacement equations. Wei and Dharani [8] present a study about sandwich plates composed of outer layers of glass and the core of PVB. For this analysis, a sandwich plate with 1m x 1m was subjected to blast load, whose parameters are overpressure p_{max} = 6894.8 Pa, time duration of positive phase t_d = 0.0077 s and decay coefficient *a'* = 0.55. Both materials,

glass and PVB, were considered in this model as isotropic. The properties of glass and PVB are shown in Tab. 2. In addition, Wei and Dharani [8] showed that PVP material is characterized by two types of shear modulus, i.e., a short-term shear module (G_0) and a long-term shear module (G_∞). Considering the total time of this analysis is sufficiently small, only G_0 was used as shear module.

Table 2. Characteristics of structure, Wei and Dharani [8]

Data	Glass	PVB
h_i (m)	0.00476	0.00152
$E_1 = E_2$ (GPa)	72	0.98
$G_{12} = G_{13} = G_{23}$ (GPa)	28,8	-
G_0 (GPa)	-	0.33
$\nu_{12} = \nu_{13}$	0.25	0.4918
ρ (kg/m³)	2500	1100

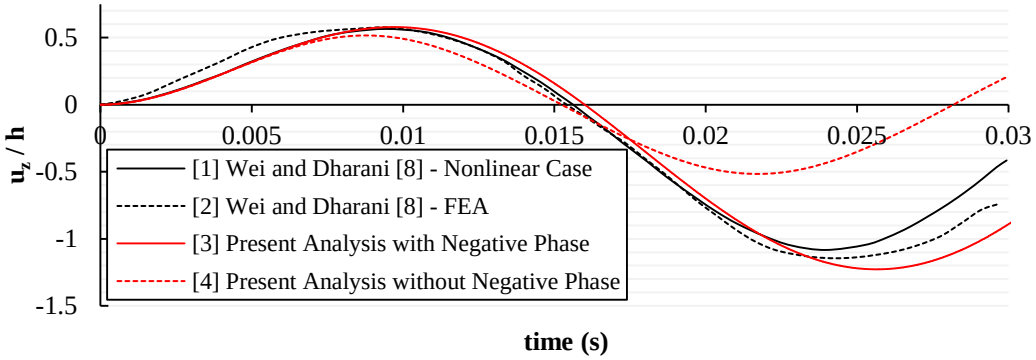

Figure 2. Midpoint displacement x time, Wei and Dharani [8]

Fig. 2 shows the results obtained by Wei and Dharani [8], curves [1] and [2], and the other ones obtained by the present work, curves [3] and [4]. The first curve represents the nonlinear analysis using the mathematical model by Wei and Dharani [8], where the maximum displacement occurs in u_z/h = -1.083221 when t = 0.023966s. The second curve is a finite element model, also developed by Wei and Dharani [8], to compare with the curve [1]. In this case, this model shows the maximum displacement in u_z/h = -1.139249, when t = 0.024924s. The third curve is the present mathematical model considering the negative phase in the analysis, the maximum displacement is registered in u_z/h = -1.227630 when t = 0.025643s. Finally, curve [4] is a representation of the same analysis without the negative phase. The results obtained is a maximum displacement u_z/h = -0.516321, when t = 0.021710s.

The response of the structure is shown in Fig. 2. It is possible to observe that there is a curve, [3], that considers the negative phase and another, [4], which only considers the positive phase and this one results in a maximum relation uz/h = -0.5163, while the first one uz/h = -1.2276.

For the parametric analysis, the Excel Solver was used to find ideal values of Z and W_{TNT} based on the loading information presented in Tab. 2. In this way, the results obtained were W_{TNT} = 2.62 kg and Z = 23.168 m/kg$^{1/3}$.

Fig. 3 (a) shows the behavior of the structure when subjected to explosive loads (including the negative phase) between W_{TNT} = 10 kg and W_{TNT} = 100 kg. Considering this case, the ratio $|u_z/h|$ for W_{TNT} = 2.62 kg, W_{TNT} = 10 kg, W_{TNT} = 20 kg, W_{TNT} = 40 kg, W_{TNT} = 60 kg, W_{TNT} = 80 kg and W_{TNT} = 100 kg where Z = 23.168 m/kg$^{1/3}$, are $|u_z/h|$ = 1.389113, $|u_z/h|$ = 1.578581, $|u_z/h|$ = 1.586943, $|u_z/h|$ = 1.601907, $|u_z/h|$ = 1.699387, $|u_z/h|$ = 1.768155 and $|u_z/h|$ = 1.819792, respectively. These $|u_z/h|$ cause, in relation to W_{TNT} = 2.6225 kg, a difference corresponding to13.63%, 14.24%, 15.31%, 22.33%, 27.28% and 31% in this order.

In the same way, an evaluation for $|u_z/h|$ based on W_{TNT} for different Z values, as shown in Fig. 3 (b). As expected, smaller values of scalar Z distances (m/kg$^{1/3}$) present the largest displacements $|u_z/h|$. Therefore, based on the recurrence of Fig. 3 (a), it is possible to determine a characteristic equation of this plate, that is, a relation between u_z/h, Z, and W_{TNT}, where Z and W_{TNT} are the input data. Based on this, the representative expression of the plate of Wei and Dharani [8] is given by Equation (13).

Equation (13) presents the main behavior of the curves shown in Fig. 3 (a) corresponds to a 5th degree polynomial function and the recurrences of the coefficients of each parameter Z^i are well represented by a 3th degree polynomials function. Furthermore, it is verified that this equation is numerically determined since the solution of the system of differential equations problem is given by Runge-Kutta, a numerical solution.

Dynamic Amplification Factor (DAF), the behavior of the structure of Wei and Dharani [8] considering Z = 23.168 m/kg$^{1/3}$. The configuration of the DAF curvature is performed based on the load variation, Fig. 4. An interesting point to note corresponds to the peaks present in the DAF graph, in which Reis [13] and Reis et al. [15] show that such an increase may be the prominence of the effect of the negative phase in relation to the positive phase or the presence of resonance. This process is observed when the two curves are compared, considering or not the negative phase, in Fig. 4. In this case, considering specific values of TNT mass, scalar distance, and the physical-geometric characteristics of the structure, the highest displacement, in absolute numbers, occurs during the negative phase.

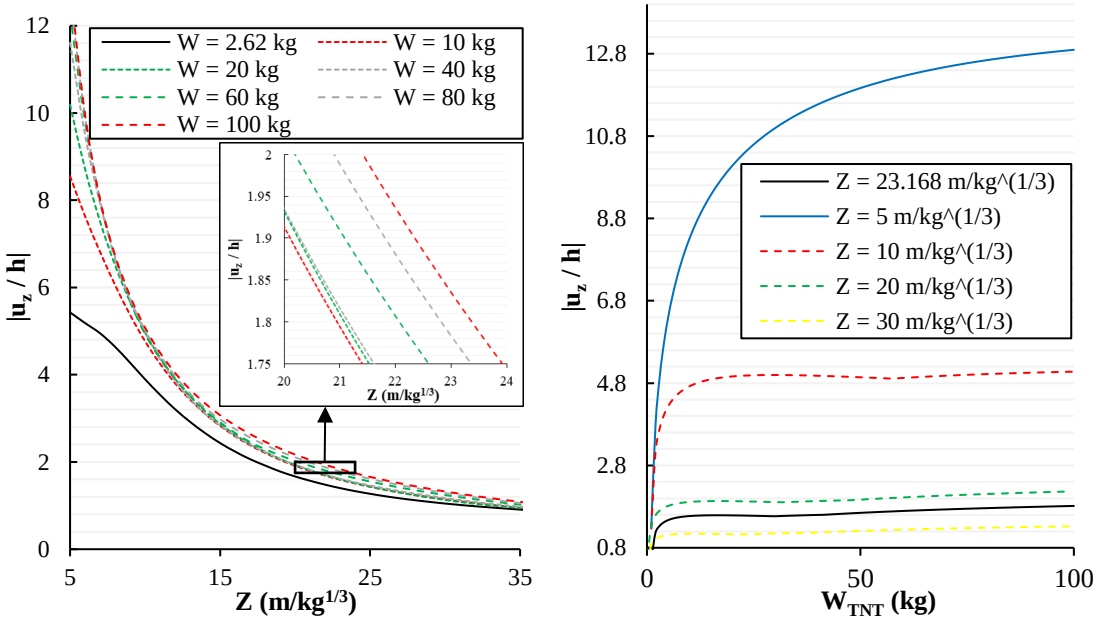

Figure 3. (a) ratio u_z / h versus Z (b) ratio u_z / h versus W_{TNT}

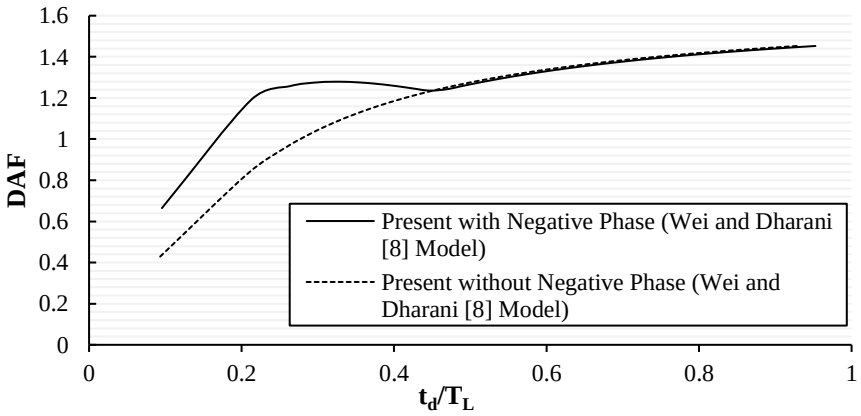

Figure 4. DAF versus t_d / T_L

$$\frac{u_z}{h} = aZ^5 + bZ^4 + cZ^3 + dZ^2 + eZ + f$$

$$\begin{bmatrix} a \\ b \\ c \\ d \\ e \\ f \end{bmatrix} = \begin{bmatrix} -3.670\times10^{-12} & 1.145\times10^{-9} & -1.369\times10^{-7} & 1.122\times10^{-6} \\ 5\times10^{-10} & -1\times10^{-7} & 2\times10^{-5} & -0.0001 \\ -2\times10^{-8} & 7\times10^{-6} & -0.0008 & 0.0045 \\ 6\times10^{-7} & -0.0002 & 0.0175 & -0.0631 \\ -7\times10^{-6} & 0.0019 & -0.1908 & -0.1046 \\ 4\times10^{-5} & -0.0089 & 0.8027 & 8.5545 \end{bmatrix} \begin{bmatrix} W_{TNT}^3 \\ W_{TNT}^2 \\ W_{TNT} \\ 1 \end{bmatrix} \tag{13}$$

4 Conclusions

This work aims to present the nonlinear behavior of laminated plates subjected to explosive loading, considering plate theories already established in the literature.

The process of determining the governing equations was performed using Hamilton's method, applying the expressions of internal and external energies of the structure. The solution used corresponds to the application of the Fourier series for simply supported plates. In the solution of the system of differential equations, the Runge-Kutta method is the best and most applied, since such equations are highly nonlinear.

Considering an example of a laminated plate subjected to explosion present in the literature, this work improved the research by performing a parametric analysis to understand how the structure used would behave through the variation of loading parameters. Verified, based on this, that the plate has a similar behavior for each variation of explosive mass, being able to generate an equation that correlates the maximum displacement of the structure with the two main explosive parameters. Finally, in the DAF evaluation, it becomes evident that the consideration of the negative phase is essential since for low values of t_d/T_L, where the difference in results between the use and non-use of the negative phase becomes expressive. However, more studies are necessary to confirm if this case is characterized using negative phase or if there is the presence of resonance.

Acknowledgements. This study was financed in part by the Coordenação de Aperfeiçoamento de Pessoal de Nível Superior – Brasil (CAPES) – Finance Code 001 and FAPERJ – Grant Number E-26/010.002150/2019.

Authorship statement. The authors hereby confirm that they are the sole liable persons responsible for the authorship of this work and that all material that has been herein included as part of the present paper is either the property (and authorship) of the authors or has the permission of the owners to be included here.

References

[1] Friedlander, F.G. The diffraction of sound pulses I. Diffraction by a semi-infinite plane. Communicated by G. I. Taylor, F.R.S., 1940.
[2] Granström, S.A. Loading characteristics of fair blasts from detonating charges. Technical Report 100, Transactions of the Royal Institute of Technology, Stockholm, 1956.
[3] US Department of Defense. Structures to resist the effects of accidental explosions, US DoD, Washington DC, USA, UFC-3-340-02, 2008.
[4] Rigby, S. E., Andrew, T., Bennett, T., Clarke, S. D., Fay, S. D. The Negative Phase of the Blast Load. International Journal of Protective Structures 5(1):1-19, 2013.
[5] Rigby, S.E. Blast Wave Clearing Effects on Finite - Sized Targets Subjected to Explosive Loads. Ph. D. Thesis. Department of Civil and Structural Engineering, University of Sheffield, UK, 2014.
[6] Gupta, A.D., Gregory, F.H., Bitting, R.L., Bhattachary, S. Dynamic Analysis of an Explosive Loaded Hinged Rectangular Plate. Pergamon Journal Ltd, Computers & Structures 26339-344, 1987.
[7] Librescu, L., Nosier, A. Response of Laminated Composite Flat Plates to Sonic Boom and Explosive Blast Loadings. American Institute of Aeronautics and Astronautics, 1990.
[8] Wei, J., Dharani, L. R. Response of laminated architectural glazing subjected to blast loading. International Journal of Impact Engineering 32(12):2032-2047, 2006.
[9] Kazanci, Z., Mecitoglu, Z. Nonlinear Dynamic Behavior of Simply Supported Laminated Composite Plates Subjected to Blast Loads. Journal of Sound and Vibration, 2008.
[10] Susler, S., Turkmen, H. S., Kazanci, Z. The Nonlinear Dynamic Behavior of Tapered Laminated Plates Subjected to Blast Loading. Shock and Vibration, 2012.
[11] Amabili, M., Balasubramanian, P., Garziera, R., Royer-Carfagni, G. Blast Loads and Nonlinear Vibration of Laminated Glass Plates in an Enhanced Shear Deformation Theory. Composite Structures, v. 252, 2020.
[12] ASCE, American Society of Civil Engineers. Structural Design for Physical Security. ASCE Manuals and Reports on Engineering Practice N° 142. Structural Engineering Institute, 2021.
[13] Reis, A.W.Q.R. Dynamic analysis of plates subjected to blast load. M. Sc. Dissertation (in Portuguese), Rio de Janeiro State University, Brazil, 2019.
[14] Reis, A.W.Q.R., Burgos, R.B., Oliveira, M.F.F. Blast Wave Analysis in Plate Structures Considering Membrane Effect, Proceedings of the Ibero-Latin American Congress on Computational Methods in Engineering, Natal/RN, Brazil, 2019.
[15] Reis, A.W.Q.R., Burgos, R.B., Oliveira, M.F.F. Nonlinear Dynamic Analysis of Plates Subjected to Explosive Loads, Latin American Journal of Solids and Structures, 2022.
[16] Reddy, J. N. Mechanics of Laminated Composite Plates and Shells Theory and Analysis, 2nd ed, 2003.
[17] Mendonça, P.T.R. Materiais Compostos & Estruturas-Sanduíche: Projeto e Análise. Editora Orsa Maggiore, 2a edição. Florianópolis – Brazil, 2019.